Available online at www.sciencedirect.com

SciVerse ScienceDirect

Geochimica et Cosmochimica Acta 105 (2013) 455–471

Geochimica et Cosmochimica Acta

www.elsevier.com/locate/gca

Isotopic and hydrologic responses of small, closed lakes to climate variability: Comparison of measured and modeled lake level and sediment core oxygen isotope records

Byron A. Steinman [a,*], Mark B. Abbott [a], Daniel B. Nelson [b], Nathan D. Stansell [c], Bruce P. Finney [d,e], Daniel J. Bain [a], Michael F. Rosenmeier [a]

[a] Department of Geology and Planetary Science, University of Pittsburgh, Pittsburgh, PA, United States
[b] School of Oceanography, University of Washington, Seattle, WA, United States
[c] Byrd Polar Research Center, The Ohio State University, Columbus, OH, United States
[d] Department of Geosciences, Idaho State University, Pocatello, ID, United States
[e] Department of Biological Sciences, Idaho State University, Pocatello, ID, United States

Received 5 October 2011; accepted in revised form 15 November 2012; available online 1 December 2012

Abstract

Simulations conducted using a coupled lake-catchment isotope mass balance model forced with continuous precipitation, temperature, and relative humidity data successfully reproduce (within uncertainty limits) long-term (i.e., multidecadal) trends in reconstructed lake surface elevations and sediment core oxygen isotope ($\delta^{18}O$) values at Castor Lake and Scanlon Lake, north-central Washington. Error inherent in sediment core dating methods and uncertainty in climate data contribute to differences in model reconstructed and measured short-term (i.e., sub-decadal) sediment (i.e., endogenic and/or biogenic carbonate) $\delta^{18}O$ values, suggesting that model isotopic performance over sub-decadal time periods cannot be successfully investigated without better constrained climate data and sediment core chronologies. Model reconstructions of past lake surface elevations are consistent with estimates obtained from aerial photography. Simulation results suggest that precipitation is the strongest control on lake isotopic and hydrologic dynamics, with secondary influence by temperature and relative humidity. This model validation exercise demonstrates that lake-catchment oxygen isotope mass balance models forced with instrumental climate data can reproduce lake hydrologic and isotopic variability over multidecadal (or longer) timescales, and therefore, that such models could potentially be used for quantitative investigations of paleo-lake responses to hydroclimatic change.

1. INTRODUCTION

Hydrologic and isotope mass balance models have long been used to quantitatively describe lake responses to climate forcing. In early predictive models (e.g., Dinçer, 1968; Gat, 1970) the common equations describing lake water and isotope (oxygen and hydrogen) mass balance were solved at steady state using analytical methods. For many applications such steady state models are an adequate approximation of the lake system (e.g., when simulating isotopic responses to climate forcing in terminal and through-flow lakes with minimal intra- and inter-annual volumetric changes) (Gibson et al., 2002). However, when simulating transient lake responses to climate forcing or modeling more complex lake-catchment systems, steady-state approaches are not appropriate and should be replaced by non steady-state methods. To address these issues, past researchers have developed systems of ordinary or partial differential equations solved using numerical

* Corresponding author.
E-mail address: bas56@psu.edu (B.A. Steinman).

0016-7037/$ - see front matter © 2012 Elsevier Ltd. All rights reserved.
http://dx.doi.org/10.1016/j.gca.2012.11.026

methods (e.g., Hostetler and Benson, 1990, 1994; Benson and Paillet, 2002).

In seasonal hydroclimatic settings such as the Pacific Northwest, hydrologic regimes are largely controlled by dry season (i.e., summer) evapotranspiration and wet season (i.e., late fall through early spring) precipitation and changes from year to year in these climate variables. This produces large intra- and inter-annual volumetric fluxes in lake catchment systems and a persistent hydrologic and isotopic disequilibrium. Models of lakes in seasonal climates should therefore incorporate non-steady state equations that can simulate intra-annual hydrologic and isotope dynamics as well as longer-term inter-annual to multidecadal lake responses to climate change. Such models should simulate variations in the mean state (i.e., multi-decade to century) and the stochastic (i.e., random, inter-annual) variability of climate.

To achieve these objectives (i.e., simulating lake dynamics on a wide range of timescales using non-steady state methods), model complexity must be increased by adding equations, variables and parameters that provide a more detailed description of both the lake and its environmental setting. Implicitly, each component of a lake model is only an approximation of a certain aspect of lake-environment physics and as such contributes some amount of error to model simulation results. To quantify the gain (or loss) in accuracy resulting from increasing model complexity, validation experiments that account for uncertainty in the primary model variables and that involve direct comparison to observations of lake dynamics should be conducted.

This manuscript is the first (along with Steinman and Abbott, 2012) in a two part series that demonstrates how lake model simulations can be used to investigate lake hydrologic and isotopic responses to climate forcing, and how modeling exercises combined with sediment core data can potentially be used to produce probabilistic, quantitative paleo-reconstructions of specific climate variables. The development of quantitative estimates of past hydroclimatic conditions is important for establishing sound water management strategies in drought prone regions where both population and economic expansion are placing greater demands on water supplies. Producing quantitative paleo-interpretations (Steinman and Abbott, 2012) first requires validation exercises (which we present here) to ensure that model predictions of lake behavior correspond with observations (or measurements) of lake hydrologic and isotopic changes. The overall objective of these papers is to provide a template for producing quantitative interpretations of lake sediment paleorecords, and to demonstrate how characterizing uncertainty (e.g., in physical parameters of the lake-catchment system or in climate datasets) is essential for constraining error in model predictions of lake geochemical dynamics.

The model experiments presented here build upon the work of Steinman et al. (2010a,b) as well as many other climate modeling studies (e.g., Donovan et al., 2002; Jones et al., 2005; Shapley et al., 2008) and are intended to establish a general method for validating model isotopic and hydrologic predictions through comparison to measured sediment core oxygen isotope values and lake level changes. As part of this study, we reconstruct recent lake surface elevations and sediment (i.e., endogenic and biogenic carbonate mineral) oxygen isotope values ($\delta^{18}O$) in Castor and Scanlon Lakes, north-central Washington using a modified version of the lake-catchment hydrologic and isotope mass balance model of Steinman et al. (2010a). Model simulations were conducted using continuous temperature and precipitation datasets spanning the instrumental period (1900–2007) and validated using georeferenced aerial photographs and lake sediment core records. Uncertainty in model simulations was imparted by several factors including the timing of carbonate mineral formation (for which limited observational data exist) and small climatic differences between Castor Lake and the nearby weather stations applied in this study. To account for these uncertainties, we conducted a series of Monte Carlo simulations in which climate data and the timing of carbonate mineral formation were randomly varied within limits defined by statistical analysis and observations of other, similar lakes, respectively.

2. METHODS

2.1. Study sites and regional climate

Scanlon Lake (SL) (48.542N, 119.582W) and Castor Lake (CL) (48.539N, 119.561W) are located in north-central Washington on a bedrock plateau adjacent the Okanogan River (Figs. 1 and 2). This region, known as the "Limebelt", is topographically higher than the bordering river valley and is therefore isolated from regional groundwater. Both CL and SL have small catchments (<1 km^2) that are characterized by brush-steppe vegetation with evergreen and secondary deciduous forest at higher elevations. Climate in this region is seasonal and semi-arid (Fig. 3), largely controlled by the interaction between the Pacific westerlies and the Aleutian low- and north Pacific high-pressure systems. Winter precipitation and temperature are strongly influenced by ENSO (The El Niño Southern Oscillation) and the PDO (The Pacific Decadal Oscillation) (Nelson et al., 2011; Steinman et al., 2012), which makes this region particularly important for paleoclimate investigations of longer-term Pacific Ocean influences on regional water supplies. Both CL and SL are closed lakes, although CL does occasionally overflow along the northeastern shoreline during pluvial events. Additional detail on the study sites and regional climate can be found in Steinman et al. (2010a).

2.2. CL sediment core recovery and sampling

In January 2004, an undisturbed sediment–water interface core was recovered from a depth of ~11.5 m (Fig. 2) at CL using a freeze core assembly. The core was transported on dry ice to the University of Pittsburgh and sampled at 1–3 mm intervals for carbonate mineral oxygen isotope ($\delta^{18}O$) and X-ray diffraction analyses. A description of sediment core processing and analyses methods is provided by Nelson et al. (2011) and is summarized in Electronic Annex EA-1.

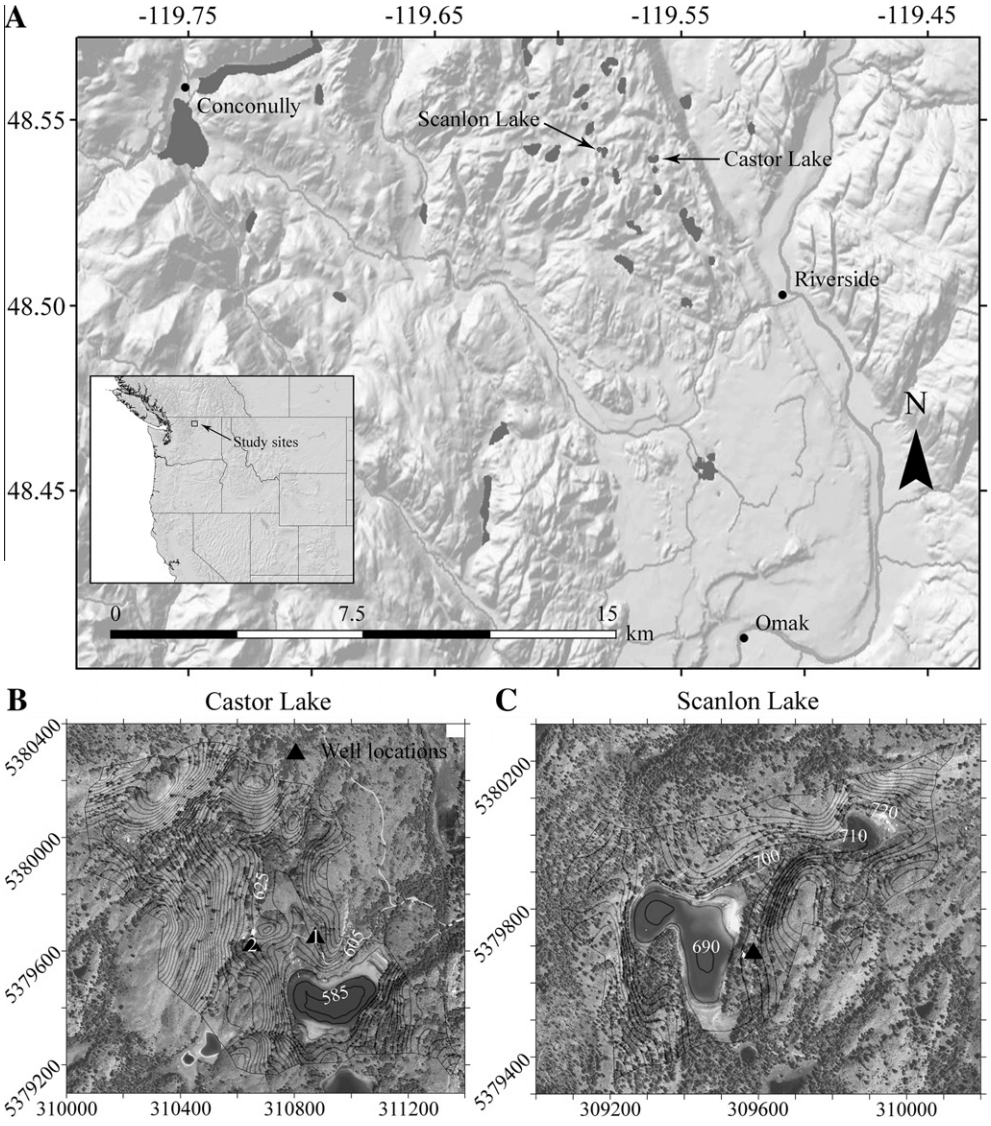

Fig. 1. Regional basemap (A) showing the location of Castor Lake and Scanlon Lake in north-central Washington, USA. Catchment topography and land cover map of Castor Lake (B) and Scanlon Lake (C) adapted from aerial photographs taken on July 1st, 2006 (Electronic Annex EA-1). Catchment maps are in UTM coordinates expressed in meters. Five meter elevation contours (above mean sea level) are displayed.

2.3. CL sediment core chronology

Near-surface sediment chronology and sediment accumulation rates were determined by ^{14}C and ^{137}Cs dating. ^{210}Pb and ^{137}Cs activities were measured at the Freshwater Institute at the University of Manitoba in Winnipeg, Canada. Details of the CL core chronology are provided by Nelson et al. (2011) and are summarized in Electronic Annex EA-1.

2.4. SL sediment core recovery and sampling

Surface sediments were collected from a depth of ~2.5 m (Fig. 2) at SL in July 2007 using a piston corer designed to retrieve undisturbed sediment–water interface profiles. The core was extruded in the field at 2 mm intervals (to a depth of 22.6 cm) by upward extrusion into a sampling tray fitted to the top of the core barrel.

Sediment samples were disaggregated in 7% H_2O_2 for ~24 h and washed through a 63 μm sieve. Coarse material (>63 μm) was collected on filter paper and dried for ~12 h at 60 °C. Adult valves of *Limnocythere staplini* ostracods were picked under magnification from the dried samples and cleaned by hand using deionized water before drying. Oxygen isotopic ratios were measured on aggregate samples of ~20 ostracod valves from each 2 mm sediment sample. Only fully intact, thoroughly clean valves without discoloration or evidence of dissolution were selected for analysis. Isotopic ratios were measured at the University of Arizona Environmental Isotope Laboratory using an automated carbonate preparation device (KIEL-III) coupled to a gas-ratio mass spectrometer (Finnigan MAT 252).

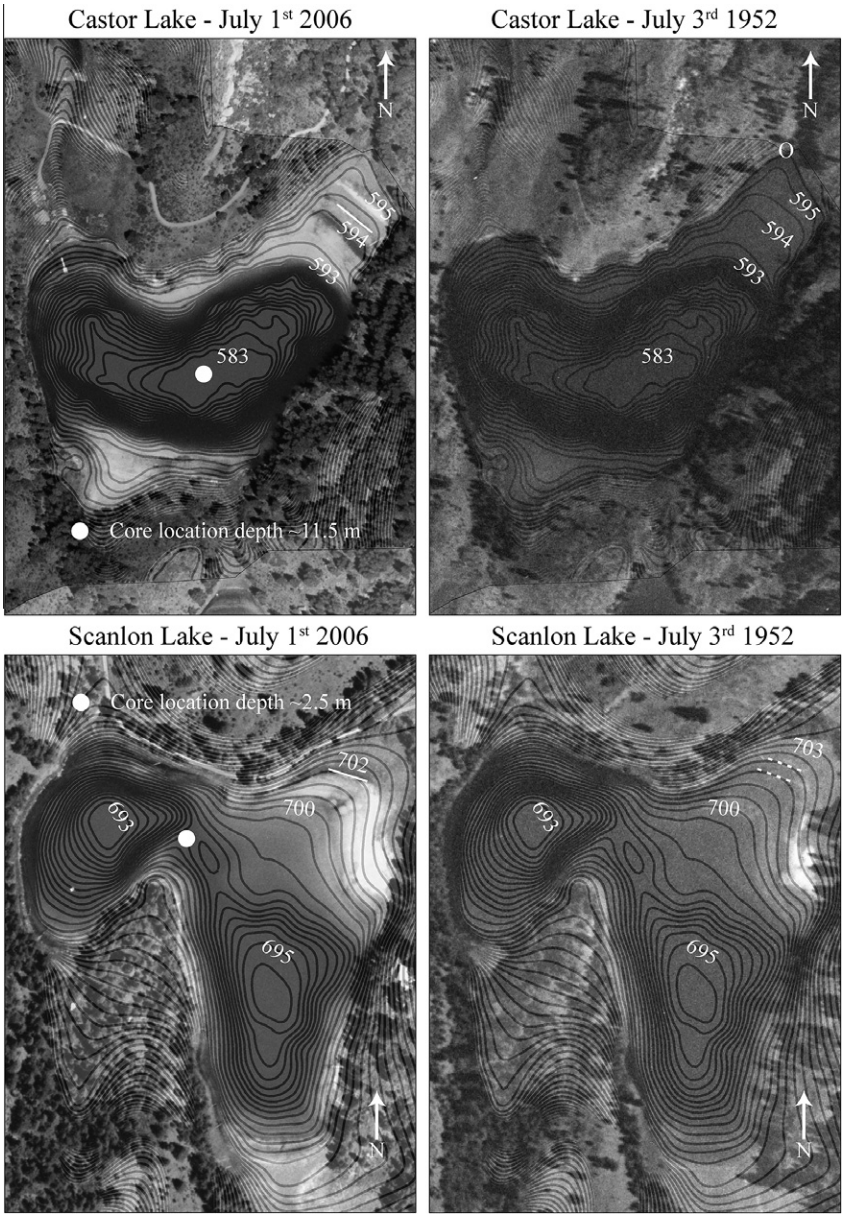

Fig. 2. Aerial photographs of Castor Lake (top) and Scanlon Lake (bottom) on 07/03/1952 and 07/01/2006 superimposed with catchment topography and lake bathymetry. The "O" in the 1952 image marks active overflow at the northeastern corner of CL. The solid lines mark lake surface elevation measurements. The dashed lines mark maximum and minimum possible lake surface elevations. Closed circles depict the coring locations. Elevation contours in 0.5 meter intervals (above mean sea level) are displayed.

Powdered samples were reacted with dehydrated phosphoric acid under vacuum at 70 °C. Due to backlogs, some samples were run at the University of Pittsburgh using a dual-inlet GV Instruments, Ltd. (now IsoPrime, Ltd.) IsoPrime stable isotope ratio mass spectrometer and MultiPrep inlet module. Isotopic values are expressed in conventional delta (δ) notation as the per mil (‰) deviation from Vienna PeeDee Belemnite (VPDB). Analytical precision (based on repeated measurements of NBS-18 and NBS-19 carbonate standard materials) was better than 0.1‰ at both laboratories for each sample run. No adjustments of $\delta^{18}O$ values were required to establish inter-laboratory consistency. X-ray diffractometry was completed at the University of Pittsburgh's Materials Micro-Characterization Laboratory using a Phillips X'Pert Powder Diffractometer over a 2θ range of 10° to 80°.

2.5. SL sediment core chronology

Sediment chronology and sediment accumulation rates at SL were determined by ^{210}Pb dating using the Constant Rate of Supply (CRS) method (Appleby and Oldfield, 1978, 1983; Oldfield and Appleby, 1984). Radioisotope (^{210}Pb, ^{137}Cs and ^{226}Ra) activities were determined by direct

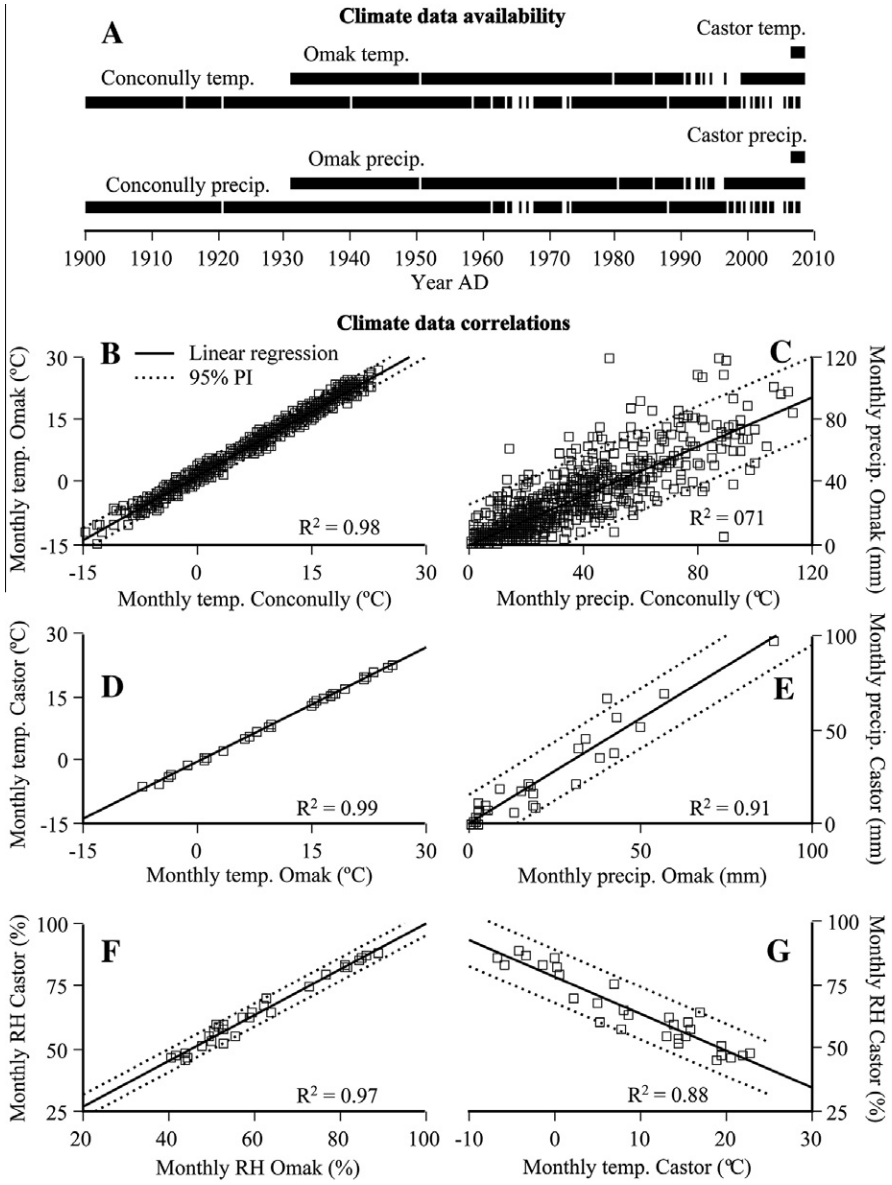

Fig. 3. Climate data availability (A) for weather stations located at Castor Lake, Omak, and Conconully. Gaps in the solid black bars depict time periods for which data are not available. Note that continuous monthly RH data spanning the time period 1989–2007 AD are available from the Omak station. Monthly temperature and precipitation data correlations between Omak-Conconully (B, C respectively) and Castor Lake-Omak (D, E respectively). Monthly RH data correlation between Castor Lake-Omak (F). Monthly RH and temperature data correlation at Castor Lake (G). Solid lines depict regression equations used to produce continuous monthly climate datasets for model application (Fig. 4). Dashed lines depict 95% prediction intervals.

gamma counting (Appleby et al., 1986; Schelske et al., 1994) using an EG & G Ortec GWL well-type intrinsic germanium detector at the University of Florida's Land Use and Environmental Change Institute. Errors in ages were propagated using first-order approximations and calculated in accordance with Binford (1990).

For the SL age model, material for radiocarbon measurements was isolated from two terrestrial macrofossil samples (24 cm and 53 cm). Analyses were conducted at the W.M. Keck Carbon Cycle Accelerator Mass Spectrometry Laboratory at the University of California, Irvine (UCI). Samples were pretreated at the University of Pittsburgh following standard acid–base-acid procedures (Abbott and Stafford, 1996). Radiocarbon ages were calibrated using the CALIB online software program version 6.0.0 (IntCal09) (Stuiver et al., 1998; Reimer et al., 2004). A more detailed discussion on SL core dating is provided in Electronic Annex EA-1.

2.6. Water chemistry

Water samples for hydrogen and oxygen isotope and ion concentration analyses were collected from the surface of SL and CL and from shallow production wells within the

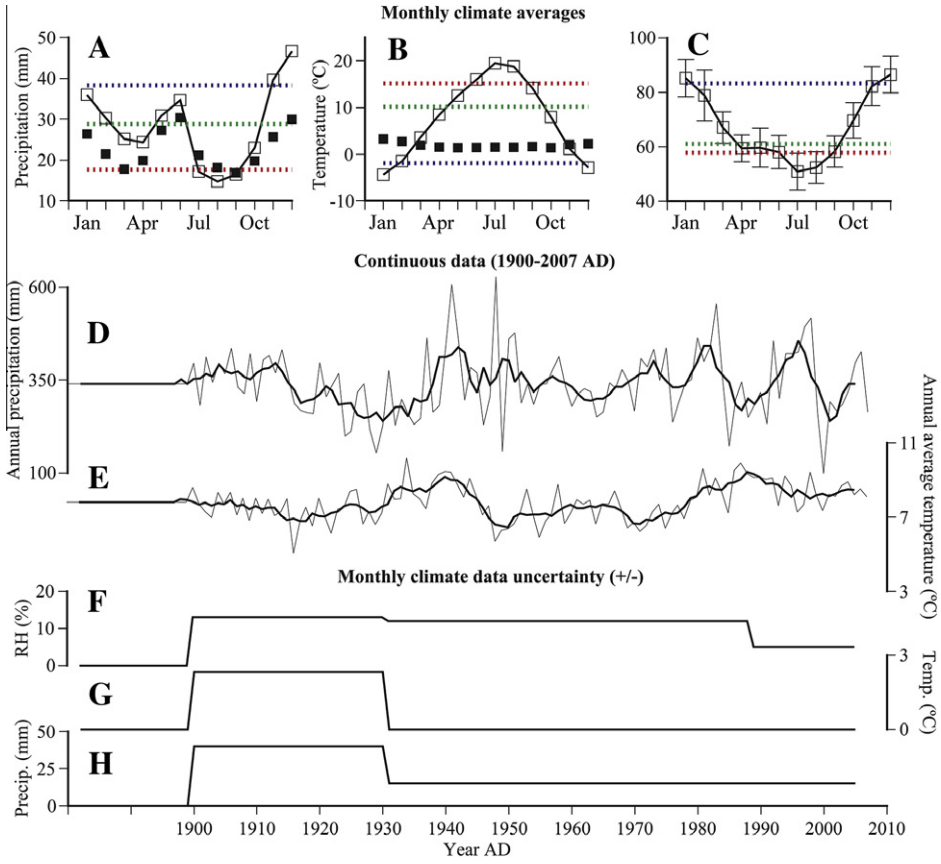

Fig. 4. Monthly average precipitation (A) temperature (B) and RH (C) for the instrumental period (1900–2007). Average November–February, March–June, and July–October values are depicted by the blue, green, and red dashed lines, respectively. Black squares (A and B) and range bars (C) depict standard deviations. Continuous precipitation (D) and temperature (E) datasets (applied in model simulations) produced using the linear regression equations depicted in Fig. 3. Uncertainty in monthly values of relative humidity (F) temperature (G) and precipitation (H) over the instrumental period. These values represent the maximum possible range (±) of variation from the estimated climate variable value in the Monte Carlo simulations. (For interpretation of the references to colour in this figure legend, the reader is referred to the web version of this article.)

lake catchments at irregular intervals between 2003 and 2011. Isotope samples were collected in 30 mL polyethylene bottles by rinsing three times with sample water and then filling and capping the bottle underwater to remove trapped air. Ion samples were filtered through acid-cleaned 0.45 μm cellulose nitrate filters to remove suspended organic and inorganic solids. Cation samples were collected in acid-washed, 125 mL polyethylene bottles and were acidified with 2 mL of ultrapure nitric acid. Anion samples were collected in 125 mL polyethylene bottles that were not acid washed. All samples were stored in a cooler immediately after sampling and kept refrigerated until analysis.

Isotopic ratios of lake water oxygen were measured at the University of Arizona Environmental Isotope Laboratory by CO_2 equilibration with a Finnigan Delta S isotope ratio mass spectrometer. For hydrogen, samples were reacted at 750 °C with Cr metal using a Finnigan H/device coupled to the mass spectrometer. The reported precision is better than 0.1‰ for $\delta^{18}O$ and 1.0‰ for δD. Elemental cation concentrations were determined using Inductively Coupled Plasma-Atomic Emission Spectrometry (ICP-AES) (Spectro Modula EOP) at the University of Pittsburgh. The estimated uncertainties (external reproducibility) for all elements was better than ±10% of measured values, based on repeated measurements of a calibration verification standard throughout the analyses. Anion species (Cl^-, F^-, SO_4^{2-} and NO_3^-) were measured on both diluted and undiluted samples by ion chromatography (IC) (Dionex ICS-2000) at the University of Pittsburgh. Estimated uncertainties on anion concentrations are less than ± 10% of measured values. Total alkalinity $\left(HCO_3^- + CO_3^{2-}\right)$ concentrations were calculated in the field by titration with 1.6N H_2SO_4 and BGMR powder indicators. Sulfate concentrations were directly measured using the IC and were inferred on the basis of molar conversion of sulfur concentrations obtained using ICP-AES.

2.7. Historical lake level estimates

Three-dimensional catchment representations for SL and CL were constructed from ⅓ arc second (~10 m resolution) National Elevation Data (NED) raster images, as well as near-lake catchment survey and bathymetric data (Fig. 1). Measurements of historical lake level were ob-

tained by overlaying eleven georeferenced aerial photographs and satellite images (dating between 1945 and 2006) onto the lake-catchment topographic-bathymetric maps (Fig. 2). Additional detail on the methods used to produce the catchment maps and historical lake level estimates can be found in Electronic Annex EA-1.

2.8. Instrumental weather datasets

Monthly precipitation and temperature datasets spanning the periods 1900–2007 and 1931–2007 were obtained from the Conconully and Omak National Climatic Data Center (NCDC) weather stations, respectively (Fig. 3). The datasets are largely continuous, although considerable gaps exist in both that prevent the exclusive use of either in model simulations. Both of these weather stations are located within 14 km and ~300 m elevation of CL and SL (Fig. 1). Monthly relative humidity (RH) data collected from 1989 to 2007 were obtained from the Pacific Northwest Cooperative Agricultural Weather Network (AgriMet) weather station (also located in Omak). In May 2006, a Campbell Scientific weather station was installed on the northwestern shoreline of CL, ~2 m above the lake surface. Since that time it has measured precipitation, temperature, RH, solar short wave radiation, barometric pressure and wind speed at 30 s intervals and recorded the average value of measurements every 30 min. Precipitation amounts were measured using a Campbell Scientific tipping bucket with an antifreeze, snowfall adaptor installed during winter months. Data collected by the CL station between May 2006 and October 2008 were post-processed to produce monthly values (i.e., data collected at 30 min intervals were averaged or, in the case of precipitation, summed).

To develop continuous century-long precipitation and temperature datasets, the monthly Conconully and Omak weather station data were adjusted on the basis of strong linear correlations to the monthly CL data (Fig. 3). Uncertainty in climate datasets was estimated on the basis of the 95% prediction limits of the linear regression equations relating climate data from different stations (Fig. 4). The reliance on the Conconully data to produce estimates for the 1900–1930 time period led to a relatively large uncertainty range in both precipitation and temperature over this interval. For example, the 95% prediction limit range of precipitation values between Conconully and Omak is ~25 mm; whereas the prediction limit range between Omak and CL is ~15 mm. The sum of these two values (±40 mm/mon), was applied over the 1900–1930 period to characterize the full range of potential uncertainty. Likewise, temperature values were most indeterminate over the 1900–1930 period although no uncertainty was assumed thereafter due to the very strong correlation (and correspondingly narrow 95% prediction limit range) between temperature at Omak and CL. Combined uncertainties (as in the 1900–1930 precipitation data) were not applied to precipitation and temperature data in the months during the 1990s when the Omak station did not record data. For all months prior to 1989, RH was calculated as a function of temperature, with uncertainties determined by the 95% temperature-RH prediction limit range. For all months after 1989, RH values were determined using the Omak AgriMet weather station data adjusted on the basis of the linear regression with the CL station data. Electronic Annex EA-1 contains additional detail on the methods applied to produce the continuous weather station datasets.

2.9. Model structure

CL and SL hydrologic and isotope dynamics were simulated using the lake-catchment model of Steinman et al. (2010a). This model describes the hydrologic and isotope mass-balance of a lake using modified forms of the following equations:

$$\frac{dV_L}{dt} = \Sigma I - \Sigma O \tag{1}$$

$$\frac{d(V_L\delta_L)}{dt} = \Sigma I\delta_I - \Sigma O\delta_O \tag{2}$$

where V_L is lake volume, ΣI and ΣO are the total surface and below ground inflows to and outflows from a lake, and δ is the isotopic composition of the inflows and outflows. The hydrologic model is defined by six separate differential equations, each corresponding to a different theoretical water reservoir (e.g., catchment groundwater, snowpack, shallow and deep lake volumes). Model sub-routines for lake stratification, soil moisture availability, snowpack, and surficial and subsurface inflow control volumetric fluxes to the reservoirs.

To accommodate overflow at CL (Fig. 2), which was not included in earlier versions of the model, a flux variable (F_{OF}) was added to the model differential equation describing the hydrologic balance of the surface lake reservoir (RES_{SL}) (see Steinman et al., 2010a, Eq. (3)):

$$F_{OF} = \begin{cases} (RES_{SL} + RES_{DL} - 424562\ \mathrm{m}^3) \times dt^{-1} & RES_{SL} + RES_{DL} > 424562\ \mathrm{m}^3 \\ 0 & RES_{SL} + RES_{DL} \leqslant 424562\ \mathrm{m}^3 \end{cases} \tag{3}$$

where RES_{DL} (deep lake reservoir) + RES_{SL} = total lake volume and 424562 m^3 represents the overflow volume at a depth of 13.46 m measured from the deepest part of the basin. The complimentary differential equation describing the oxygen isotope mass balance of RES_{SL} was also modified.

Subroutines that calculate sediment $\delta^{18}O$ values on the VPDB scale were also added to the model, in order to

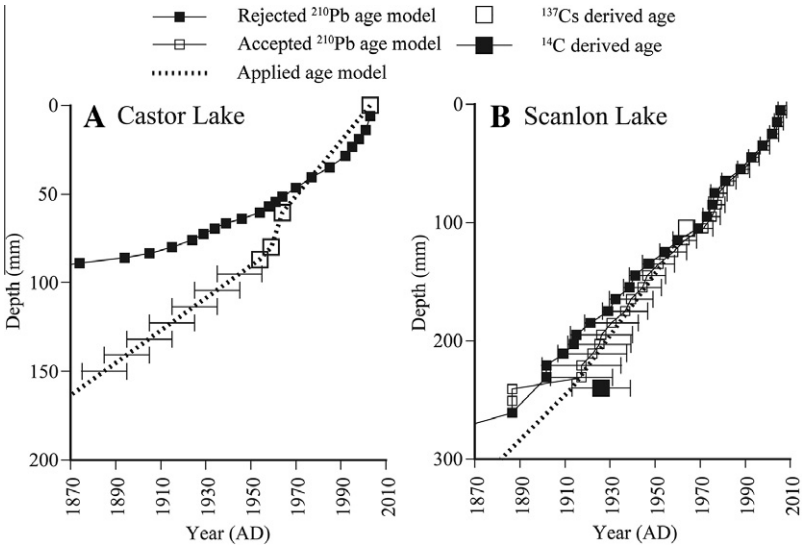

Fig. 5. Castor Lake (A) and Scanlon Lake (B) age-depth models. Small closed and open squares depict rejected and accepted ^{210}Pb dates, respectively. Large open squares depict dates inferred using ^{137}Cs. The large closed square represents a date obtained using ^{14}C. The dashed lines represent the age models applied in this study. Horizontal bars depict the estimated age model error range. Note that the applied SL age model is very similar to the accepted ^{210}Pb age model and that it passes through the 2σ error range of the ^{14}C derived age.

simulate the isotopic composition of endogenic and biogenic carbonate sediments forming at CL and SL, respectively. The CL model calculates the equilibrium fractionation factor for the aragonite water system in accordance with the equation of Kim et al. (2007):

$$1000 \ln \alpha_{Aragonite\text{-}H_2O} = 17.88(10^3 T_W^{-1}) - 31.14 \quad (4)$$

where $\alpha_{Aragonite\text{-}H_2O}$ is the equilibrium fractionation factor for aragonite and water and T_w is the water temperature in degrees Kelvin. The SL model determines the equilibrium fractionation factor for ostracod bio-calcite using the equation of Kim and O'Neil (1997):

$$1000 \ln \alpha_{Calcite\text{-}H_2O} = 18.03(10^3 T_W^{-1}) - 32.42 \quad (5)$$

where $\alpha_{Calcite\text{-}H_2O}$ is the equilibrium fractionation factor for calcite and water. In both cases values for α are related to lake water δ^{18}O values on the Vienna Standard Mean Ocean Water (VSMOW) scale in accordance with the standard isotope fractionation relationship:

$$\alpha_{Calcite/Aragonite} = \frac{1000 + \delta_C}{1000 + \delta_L} \quad (6)$$

where $\alpha_{Calcite/Aragonite}$ is the fractionation factor of either the calcite-water or aragonite-water systems, δ_C is the isotopic composition of either aragonite or calcite, and δ_L is the isotopic composition of lake water. The model converts theoretical aragonite and calcite δ^{18}O values from the VSMOW to the VPDB scale using the following standard equation:

$$\delta_{VSMOW} = 1.03092 \times \delta_{VPDB} + 30.92 \quad (7)$$

The SL model also applies an isotopic offset of +0.8‰ (identified by von Grafenstein et al., 1999 for *L. inopinata*) to bio-calcite δ^{18}O values to simulate the vital isotopic effect associated with carapace production of the *Limnocytherid* ostracods. STELLA versions of the models with an accompanying model variable and parameter table are available as part of Electronic Annex EA-2.

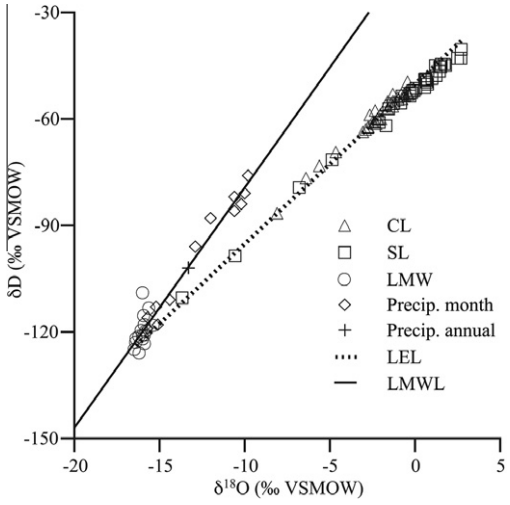

Fig. 6. Local meteoric water line (LMWL), local evaporation line (LEL), δ^{18}O and δD values for Castor Lake (open triangles) and Scanlon Lake (open squares) surface waters, local meteoric waters (LMW) (i.e., well waters from the catchments) (open circles), and monthly (open diamonds) and annual (cross) precipitation (estimated using the waterisotopes.org online calculator; Bowen and Revenaugh, 2003).

2.10. Instrumental period simulations

Model simulations utilized continuous monthly temperature, precipitation and RH datasets spanning at least part

Table 1
Castor Lake and Scanlon Lake water chemistry data.

Date	Castor Lake 5/4/06	Castor Lake 10/1/06	Castor Lake 7/26/07	Castor Well 2 8/20/07	Castor Well 1 8/20/07	Castor Lake 8/21/07	Scanlon Lake 5/04/06	Scanlon Lake 9/30/06	Scanlon Lake 7/25/07	Scanlon Lake 8/21/07
Cation mg/l										
Mg	242.8	450.2	487.3	80.7	44.4	499.5	473.9	2175.4	2124.3	2254.7
K	34.3	60.1	57	6.8	0.8	59.4	96.8	534.7	522.9	588.6
Sr	0.3	0	0.1	3.2	0.2	0.1	0.1	0.1	0.1	0.1
Al	0.1	0.1	0.2	0	0.1	0.1	0.1	1	0.1	0.1
Si	8.4	11.5	9.4	5.7	5.5	9.8	6.1	3.4	3.6	3.9
Na	87	153.3	172.8	40.1	3.3	166.9	224.3	1184.3	1252.1	1376.6
Ca	44.4	10.9	14.8	173.3	88.6	14	33.8	25.8	25	25.7
Fe	0	0	0	0	0	0	0	0.1	0.1	0
S	No data	537.4	513.2	170.8	7.1	513.3	No data	3611.1	3271.8	3487
Anion mg/l										
F	0.4	0.6	0.3	0.3	0.1	0	0	0	0	0
Cl	12.9	22.7	21.3	2	0.8	36.7	34.8	161.4	135.5	136.2
SO_4	901.2	1594.9	1461	455.8	22.2	1522.2	2179.3	10368.3	9070.5	9706.4
NO_3	0	0	0	1.2	3.2	0	0	0	0	0
ALK*	450	550	560	303	331	575	485	1100	1090	1130
TDS	1781.8	2854.3	2784.2	1072.1	500.2	2883.7	3534.2	15554.5	14224.2	15222.3
Cation meq/l										
Mg	20	37	40.1	6.6	3.7	41.1	39	179	174.8	185.5
K	0.9	1.5	1.5	0.2	0	1.5	2.5	13.7	13.4	15.1
Sr	0	0	0	0.1	0	0	0	0	0	0
Al	0	0	0	0	0	0	0	0.1	0	0
Si	0.6	0.8	0.7	0.4	0.4	0.7	0.4	0.2	0.3	0.3
Na	3.8	6.7	7.5	1.7	0.1	7.3	9.8	51.5	54.5	59.9
Ca	2.2	0.5	0.7	8.6	4.4	0.7	1.7	1.3	1.2	1.3
Fe	0	0	0	0	0	0	0	0	0	0
Anion meq/l										
F	0	0	0	0	0	0	0	0	0	0
Cl	0.4	0.6	0.6	0.1	0	1	1	4.6	3.8	3.8
SO_4	18.8	33.2	30.4	9.5	0.5	31.7	45.4	215.8	188.8	202.1
NO_3	0	0	0	0	0.1	0	0	0	0	0
SO_4**	No data	33.5	32	10.6	0.4	32	No data	225.2	204	217.5
ALK*	9	11	11.2	6.1	6.6	11.5	9.7	22	21.8	22.6
Mg/Ca	9.1	74.0	57.3	0.8	0.8	58.7	22.9	137.7	145.7	142.7
ALK/Ca	4.1	22.0	16.0	0.7	1.5	16.4	5.7	16.9	18.2	17.4
Ln(ALK/Ca)	1.4	3.1	2.8	−0.3	0.4	2.8	1.7	2.8	2.9	2.9
Charge balance										
Cat/An	0.98	1.04	1.2	1.13	1.21	1.16	0.95	1.01	1.14	1.15
Cat/An**	No data	1.03	1.15	1.05	1.21	1.15	No data	0.98	1.06	1.07

* Alkalinity measurements expressed in terms of equivalent $CaCO_3$ (mg/l) and CO_3^{2-} (meq/l).
** SO_4 concentration inferred from S data. Cat/An** calculated using SO_4 derived from S data.

of the instrumental period (Fig. 4) as inputs to reconstruct lake hydrologic and isotopic variations for comparison to measurements of lake level change and sediment core oxygen isotope values. To simulate climate variables for which no long-term (i.e., multidecadal) continuous datasets exist (e.g., insolation and wind speed), monthly average values were applied as model inputs. In all simulations, catchment and lake parameters such as soil available water capacity were held constant. Each simulation (conducted on a monthly time step) lasted 128 years of which the first twenty were a model equilibration period in which average monthly values for all climate variables were continuously applied and the remaining 108 years represented the period 1900–2007.

To simulate uncertainty in the timing of carbonate mineral formation, the model was adapted to record either aragonite (in the case of CL) or biocalcite (in the case of SL) theoretical $\delta^{18}O$ values at a randomly chosen time between the beginning of April and the end of June and to stop recording values between the beginning of July and the end of August in each year of the simulations. The choice of April through June as the starting point was based on observations of whiting events made by local residents (in the case of CL) and a general understanding of ostracod life-cycles (in the case of SL, with important caveats noted in Section 3.5, below). The average of the recorded $\delta^{18}O$ values was then applied as the carbonate mineral $\delta^{18}O$ value for that simulation year. For both CL and SL, one-hundred model simulations were conducted in which climate data (Figs. 3 and 4) and the timing of carbonate mineral formation were randomized (within statistically and seasonally defined limits, respectively) to account for the effect of uncertainty in these variables on simulated lake level and sediment $\delta^{18}O$ values over the instrumental period (1900–2007). Unless otherwise noted, all modeled lake surface elevation, depth, and $\delta^{18}O$ values discussed herein represent the average of an ensemble of one-hundred distinct model simulations.

3. RESULTS AND DISCUSSION

3.1. CL age model

The ^{210}Pb age model for CL produced using the CRS method does not include the ^{137}Cs peak at 1964 within a 2σ error range (Oldfield and Appleby, 1984) (Fig. 5). It is unlikely that ^{137}Cs is mobile at CL, given the relatively low organic matter content (10–20%) in the upper sequence of the core and the well preserved laminations (see Electronic Annex EA-1 for images of the CL and SL sediment cores, age model data tables, and supplementary discussion on age model justification). The ^{137}Cs profile was therefore applied instead of the ambiguous ^{210}Pb profile to produce the upper section of the CL age model. The estimated error range for the time period 1900–1950 is ±10 years on the basis of estimated error in the SL age model and differences in the ages of modeled and measured variations in CL aragonite $\delta^{18}O$ values.

3.2. SL age model

Calibration of the uppermost radiocarbon sample (24 cm) produced 5 possible ages, of which only one passed through the 2σ error ranges of the CRS derived ^{210}Pb dates. Therefore, to produce the SL age model, a linear function was applied to connect the ^{137}Cs peak at 10.5 cm with the minimum possible age within the 2σ error range of the radiocarbon sample at 24 cm (Fig. 5). This linear function passes through the 2σ error ranges of all ^{210}Pb measurements below 10.5 cm, and therefore represents the best possible compromise between the ^{210}Pb and ^{14}C data. An additional linear function was applied that connects the estimated age at 24 cm with the radiocarbon date at 54 cm to extend the age model through 1900. Support for the SL age model is provided by an additional ^{210}Pb chronology developed by assuming very small, non-zero unsupported ^{210}Pb activities for several of the lowermost samples (Electronic Annex EA-1).

It is difficult to determine why the ^{210}Pb measurements of SL sediment produced a reasonable age model when the ^{210}Pb data from the CL core did not, although differences in coring and sediment processing methods may have played a role. For example, CL ^{210}Pb samples were obtained from a freeze core (rather than extruded, bagged sediments in the case of SL) which could have produced inaccurate bulk density measurements, on which the CRS method relies heavily to produce an accurate age model (Oldfield and Appleby, 1984). Differences in sediment composition, density, and rates of deposition may also account for some of the discrepancy in ^{210}Pb geochemistry between the two sites.

3.3. Water chemistry measurements

CL and SL water sample isotopic values exhibited considerable seasonal variability (with $\delta^{18}O$ values ranging from −0.4 to −8.1‰ for CL and −13.7 to 2.7‰ for SL) and plot on a local evaporation line with a slope of ~4.3 (Fig. 6). SL waters were in almost all cases more isotopically enriched than CL waters collected on the same or similar dates (Electronic Annex EA-1) indicating that SL has a higher degree of hydrologic closure than CL. The approximate water table depths in CL Well 1, CL Well 2, and the SL well were 8.5 m, 17 m, and 2.5 m below the well surface, respectively, which correspond to elevations that are hydraulically upgradient from CL and SL. Isotopic values of waters collected from the wells plot at the intersection point of the local evaporation line (LEL) and the local meteoric water line (LMWL) (estimated using the values of Bowen and Revenaugh, 2003; waterisotopes.org), reinforcing the assertion that both lakes experience significant evaporative losses, in accordance with results from other, similar sites (Henderson and Shuman, 2009). The coherence between isotopic values of CL and SL catchment groundwater and theoretical meteoric values (suggested by the LMWL) indicates that no substantial isotopic enrichment of catchment groundwater occurs as a result of surficial evaporation from soils.

In accordance with the water isotope results, ion concentrations were higher at SL (which has summer TDS values of ~15,000 mg/L) than at CL (which has summer TDS values of ~2700 mg/L) (Table 1). The proportional ion composition of both lakes is similar as well, indicating that CL and SL evolve along a common solute pathway that produces high alkalinity and Ca^{2+} limitation for carbonate mineral precipitation (Eugster and Jones, 1979). This may be due in part to alkalinity generation resulting from the bacterial reduction of SO_4^{2-} in the water column (note that both CL and SL bottom water smelled strongly of H_2S in each year of the study). Water samples collected from wells in the CL catchment have higher Ca^{2+} concentrations and lower alkalinity values than the lake water, further supporting these assertions. The lack of isotopic enrichment in CL well water combined with ion concentrations and compositions that are not reflective of fresh, meteoric water (i.e., well waters contained substantial TDS concentrations) suggests that catchment waters likely acquire dissolved solids when passing through soils into the catchment aquifer. Notably, the disparity between CL well water ion concentrations indicates a lack of spatial homogeneity in the solute composition of CL catchment water. A piezometer based sampling and groundwater level monitoring program would provide a more thorough understanding of catchment hydrology and groundwater composition (including the source of the SO_4^{2-}) and could potentially provide a dataset with which to validate future model predictions of CL and SL salinity responses to climate forcing.

3.4. CL endogenic carbonate formation

At CL, aragonite precipitation from the water column likely occurs in the spring and early summer (April–August) as a result of physico-chemical and climatic control of the aragonite solubility product (K_{sp}) and Ca^{2+} ion concentrations and through biological control of dissolved inorganic carbon (DIC) equilibria and carbonate species concentrations. Aragonite precipitates when the degree of saturation (Ω) exceeds a value of one:

$$\Omega = \frac{a_{Ca} a_{CO_3}}{K_{sp}} > 1 \quad (8)$$

where a represents the ion activity of either Ca^{2+} or CO_3^{2-}. If seed crystals are not present in solution, however, aragonite precipitation will not occur until a critical level of supersaturation is reached at which the formation energy of new phase aragonite is exceeded (Koschel et al., 1983; Raidt and Koschel, 1988; Koschel, 1997).

Climate can influence aragonite formation through seasonal and inter-annual temperature and precipitation amount variations. Temperature influences aragonite formation via two interrelated mechanisms: first, by controlling K_{sp} (higher temperatures result in lower K_{sp} values), and second, through control of primary productivity, which typically increases at higher temperatures resulting in removal of CO_2 and an increase in pH (with a corresponding shift in the DIC equilibria toward the CO_3^{2-} species) (Kelts and Hsu, 1978). Rain/snowfall amounts can influence aragonite formation by controlling the delivery of Ca^{2+} ions to the lake through runoff and baseflow (Shapley et al., 2005). In Ca^{2+} limited lakes similar to CL (Table 1), carbonate production is limited by Ca^{2+} ion concentrations (Sanford and Wood, 1991) such that increased rain/snowfall results in larger Ca^{2+} ion fluxes to the lake and consequently greater ion availability for endogenic carbonate mineral production in the water column.

The biological mechanism that relates aragonite precipitation and primary productivity is not entirely understood but is thought to involve a combination of the both direct and indirect influences of picoplankton. In the former case, picoplankton blooms can alter pH and induce inorganic mineral precipitation. In the latter case, they can provide nucleation points that reduce the formation energy of aragonite crystals (Thompson et al., 1997; Hodell et al., 1998; Sondi and Juracic, 2010). At CL, biomediated aragonite formation therefore most likely occurs in the late spring after ice breakup and the initiation of thermal stratification of the water column. Subsequently, aragonite forms throughout the summer months as a result of physicochemical effects including evaporative concentration of Ca^{2+} and DIC species until the Ca^{2+} concentration drops below the saturation level (see Section 2.10).

XRD results indicate that aragonite is the only detectable carbonate mineral in the CL sediment and therefore that $\delta^{18}O$ variations in the CL core are not a result of changes in the carbonate mineral composition (Nelson et al., 2011). Further, the oxygen isotopic composition of endogenic carbonate material captured by a sediment trap deployed in CL at a depth of ~8 m from July 2005 through May 2006 (Nelson et al., 2011) is similar to both measured values from the sediment core and theoretical estimates predicted by model simulations (see Section 3.9, below), indicating that the proposed spring/summer aragonite precipitation mechanism is likely valid.

3.5. SL biogenic carbonate formation

XRD analysis of SL sediment revealed mixed carbonate mineralogy, which complicates the use of endogenic carbonates for reconstructions of lake water oxygen isotope composition. Instead, ostracod carapaces, which are abundant in SL sediment, were used for isotopic analyses. Ostracods of the species *Limnocythere staplini* were identified on the basis of carapace morphology (using SEM imagery) and studies of ostracod water chemistry tolerances (Smith, 1993; Curry, 1999; NANODe online database). A more detailed discussion of methods used to identify the species living at SL (including the SEM imagery) can be found in Electronic Annex EA-1.

Ostracod molting and reproductive cycles are triggered by changes in water temperature, food availability, and solute composition and concentration. At SL, *L. staplini* most likely hatch in the spring, molt and shed their calcite carapaces eight times until reaching adulthood in the late spring/early summer, although this cannot be confirmed without direct observation of the ostracod life cycle over at least a year. *Limnocytherids* form carapaces quickly, typically over several hours (up to 24 h in some cases), and proceed through growth stages to adulthood within 4–6 weeks

(Palacios-Fest et al., 2002). The short life cycle of *Limnocytherids* can potentially lead to several generations in one year, although the high alkalinity (>10 meq/L) and sulfate (>100 meq/L) concentrations of SL waters likely inhibits their growth past late summer.

All ostracod species form carapaces in isotopic disequilibrium with surrounding water, with an approximately constant isotopic offset (or vital effect) from the equilibrium $\delta^{18}O$ value that is largely temperature and instar independent (see Eqs. (5)–(7), above) (von Grafenstein et al., 1999). Studies have demonstrated (De Deckker et al., 1999; Ito and Forester, 2009), however, that geochemical variability in ostracod carapaces can occur even in controlled, in vitro experiments, suggesting that this isotopic offset likely varies (albeit by a small amount) in nature. For *Lymnocythere inopinata* von Grafenstein et al. (1999) determined a value of ~0.8‰, which we apply here to the SL ostracods, in light of the observed consistency between vital offsets within other families and genera.

3.6. Modeled carbonate mineral formation

The model algorithms that simulate the timing of carbonate mineral formation at SL and CL are undoubtedly oversimplified, as aragonite formation in the water column and ostracod reproduction and molting cycles are largely temperature and water chemistry dependent. By randomizing this process, however, a large proportion of the uncertainty contributed by the timing of carbonate mineral formation is accounted for in model simulations, a much better alternative than assuming constant carbonate mineral formation over a specific time range in each year. Future efforts could focus on applying temperature or water chemistry controls to the timing of carbonate mineral formation in the model structure, collecting additional material using sediment traps to provide a more robust observational dataset at CL, and directly monitoring the ostracod life cycle at SL.

3.7. Comparison of measured and modeled lake surface elevation

CL and SL lake surface elevation reconstructions based on georeferenced aerial photographs and lake-catchment contour maps demonstrate considerable variability in inter-annual water levels (Fig. 7, Electronic Annex EA-1). At CL minimum inferred lake elevation (592.5 m) occurs in 1991, with maximum lake elevation (595.5 m) during years of overflow in 1952, 1975, 1983 and 1998. At SL minimum inferred lake elevation (700 m) occurs in 1973, with maximum lake elevation (702.5 m) during 1983 and 1987. No long-term (multi-decadal) trends in lake-level change at CL or SL are apparent between 1945 and 2006. CL and SL surface elevations of 594.25 m and 701.5 m, respectively, inferred using the July 2006 orthophotograph are in both cases within 0.3 m of lake-level measurements obtained using Solinst Leveloggers (Steinman et al., 2010a).

Model experiments utilizing instrumental weather observations from 1945 to 2007 resulted in a minimum lake surface elevation (~592.2 m) at CL in 1992 and maximum values (~595.5 m) in 1952, 1975, 1983, and 1998 (Fig. 7, Electronic Annex EA-1). The average error between inferred and modeled lake surface elevation at CL was ~0.3 m with all but one inferred elevation (in the year 1945) falling within the 2σ prediction limits of model results. For SL, minimum modeled lake surface elevation (~699.3 m) was reached in 1992 with the highest lake surface elevation (~702.5 m) occurring in 1999. The average error between inferred and modeled lake volume and surface elevation at SL was ~0.5 m; however, the 1987 aerial

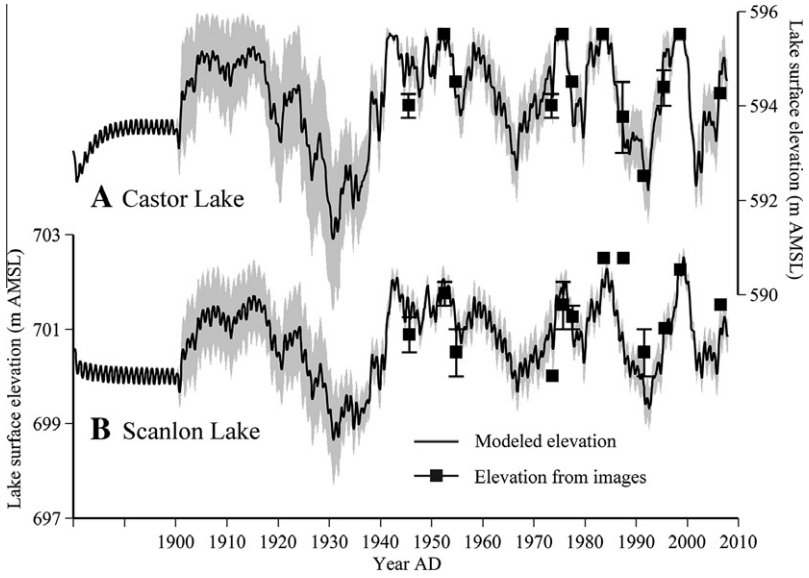

Fig. 7. Castor Lake (A) and Scanlon Lake (B) modeled (lines) and measured (squares) water surface elevations. Error bars depict maximum and minimum possible values of measured lake surface elevations. The gray shading represents the 2σ prediction intervals calculated using 100 distinct model simulations.

photograph for SL is of poor quality and is the likely reason for the exceptionally large error measured for this year. If results from 1987 are removed, the average error decreases to ~0.4 m. In all but 4 years at SL the aerial photograph inferred lake surface elevations overlapped with the 2σ prediction limits of model simulation data.

Model estimates for lake surface elevation change from 1945 to 2007 were largely consistent with observations from aerial photographs (Fig. 7, Electronic Annex EA-1) with a slightly better correspondence at CL than at SL. The reasons for the discrepancy in the predictive accuracy of the CL and SL models are not entirely clear. One potential explanation lies in the conspicuous fact that, after 1980 for SL, the model estimates for lake surface elevation are in most cases lower than observations. This underestimate could be related to several factors including inaccuracy in lake morphometry measurements (which would, in turn, lead to inaccuracy in the resulting contour maps and lake level observations) or subtle differences in precipitation, temperature, or relative humidity at the lake, relative to the weather station-derived values used within the model simulations. The latter explanation is more likely given that precipitation amounts, the most hydrologically significant climate variable in the lake models, exhibits a spatial incoherence that is uncharacteristic of temperature and RH. The relatively low correlation of the precipitation data (Fig. 3) and the correspondingly large prediction limits suggest that precipitation amounts can vary considerably on monthly timescales over short distances such as the ~14 km separating the CL and Omak weather stations, or the ~1.5 km separating CL and SL. Another possible explanation lies in the fact that SL is over 100 m higher than CL and is subject to slightly lower temperatures that result in less evapotranspiration, greater snowpack amounts, and increased spring runoff, all of which lead to higher average lake levels. These issues, coupled with the strong (relative to CL) control of evaporation on SL hydrology (Steinman et al., 2010a; Steinman and Abbott, 2012) may explain SL model underestimates of lake surface elevation after 1980.

3.8. The influence of precipitation amount and temperature on lake level

Between 1900 and 1945 (i.e., prior to the period of aerial photograph based lake level reconstruction) modeled lake levels and volumes were on average lower than during the period of observation (1945–2007) (Fig. 7), an expected result given that average annual precipitation amounts were appreciably lower prior to 1945 (Fig. 4, Electronic Annex EA-1). Model simulations predicted high lake-stands between 1940 and 1950 and lake low-stands between 1920 and 1940. In both cases, decadal average precipitation amounts were commensurate with the extent of the lake level and volume changes. For example, in the period of protracted lake low stands (1920–1940), the lowest average decadal precipitation amounts of the simulation period (1900–2007) occurred. Conversely, during the protracted high stands (1940–1950), the highest average decadal precipitation amounts of the simulation period occurred. After ~1975, simulated lake level varied between relative high and low points on an approximately decadal basis in response to roughly proportionate changes in precipitation amount.

The effect of temperature on lake level and volume is not as clear as that of precipitation. Highest average temperatures (and inferred increases in evaporation) occurred between 1980 and 1990 while the lowest lake levels occurred between 1930 and 1940 (Figs. 4 and 7). Similarly, average annual temperature over the period of observation was higher than over the period prior to observation when the lowest modeled lake surface elevations occurred. These results support the assertions of Steinman et al. (2010a) that CL and SL hydrologic variability on decadal timescales is primarily controlled by variations in precipitation amount with secondary control by temperature and RH.

For both lakes the relatively large uncertainty in precipitation, temperature, and relative humidity between 1900 and 1930 (Fig. 4) resulted in a comparatively large range of modeled depth values (Fig. 7). After ~1935 the standard deviation of depth measurements decreased substantially for SL, in response to smaller climate data prediction limits. For CL the range of modeled depth values decreased and remained largely constant after 1935 except during periods of overflow (e.g., 1952) when maximum lake level was maintained for longer periods of time. The relatively large standard deviation of modeled lake depths in the early part of the 20th century illustrates the considerable hydrologic variance imparted to lake-catchment model simulations by uncertainties in climate data.

3.9. Comparison of measured and modeled $\delta^{18}O$ records

Measured CL sediment core $\delta^{18}O$ values vary between −6.7‰ (~1960) and −3.2‰ (~1927) over the instrumental period (Fig. 8) with an average $\delta^{18}O$ value (calculated using interpolated data) of −4.9‰. For CL, model predicted annual spring/summer $\delta^{18}O$ values varied between −8.6‰ (2006) and −1.1‰ (1991) with five-year averages of the annual values reaching a minimum of −6.9‰ (1974) and a maximum of −2.8‰ (1992). The average modeled $\delta^{18}O$ value of aragonite at CL for the entire simulation period was −5.2‰, which is similar to the average value measured in sediment cores. In addition, the isotopic composition of aragonite collected using a sediment trap (Nelson et al., 2011) falls within the 2σ range of model predictions, providing additional support for model based estimates of lake sediment $\delta^{18}O$ values.

For SL, measured ostracod $\delta^{18}O$ values (without correction for a vital offset) vary between −4.9‰ (~1953) and 2.1‰ (~1926) (Fig. 8) with an average $\delta^{18}O$ value (calculated using interpolated data) of −1.2‰. Model predicted annual spring/summer $\delta^{18}O$ values ranged between −6.0‰ (1974) and 3.8‰ (1992) with five-year averages reaching a minimum of −4.1‰ (1999) and peaking at 2.5‰ (1992). The average modeled $\delta^{18}O$ value of biocalcite at SL for the entire simulation period was −1.2‰ (including the vital offset), a value that exactly matches the average value measured in sediment cores. Note that an error range estimate has been applied to all ostracod $\delta^{18}O$ values in order to account for statistical variance resulting from the

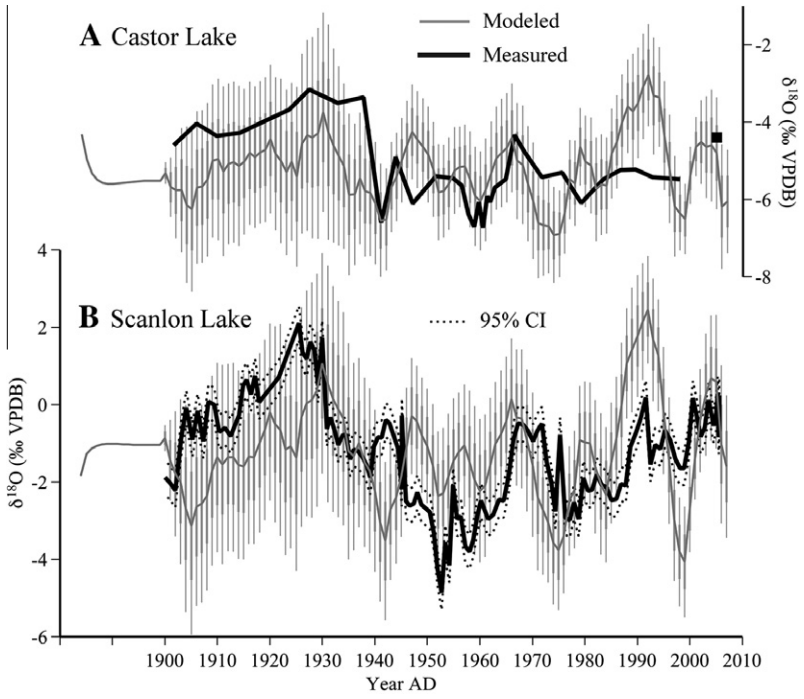

Fig. 8. Modeled (gray) and measured (black) aragonite $\delta^{18}O$ values for Castor Lake (A) and Scanlon Lake (B). Thick and thin vertical gray lines depict the 1σ and 2σ prediction intervals, respectively, of 100 distinct simulations averaged to produce the modeled values. Five year averages of modeled data are shown. The fine dashed lines in (B) depict the confidence interval for $\delta^{18}O$ measurements of Scanlon Lake ostracods. The closed square represents the average $\delta^{18}O$ value of sediment trap aragonite collected at CL in 2005–2006.

random sampling of ~20 ostracods from each sediment sample. A description of the methods used to produce this error estimate can be found in Electronic Annex EA-1.

In 77 of the 98 years of comparison, measured CL sediment core $\delta^{18}O$ values are within the 2σ uncertainly range of model predictions. For SL, a similar correspondence exists, with 74 of 106 years overlapping. Effectively, this means that one or more model realizations exist that can reproduce the majority of measured sediment core $\delta^{18}O$ variations, and therefore that the model is a reasonable approximation of the physical processes controlling lake hydrologic and isotope dynamics. Interestingly, the most notable time periods of inconsistency between measured and modeled $\delta^{18}O$ values are the same for both lakes, namely, the earliest part of both records (i.e., from 1900 to ~1935) where model predictions are consistently lower than measured values, and the 1980–1990 period in which model predictions for both CL and SL overestimate $\delta^{18}O$ values.

The generally consistent overestimation of sediment $\delta^{18}O$ by the model over the 1900–1935 time period can potentially be explained by uncertainty in precipitation, which is considerably more influential than temperature in controlling lake hydrologic and isotopic fluxes (primarily through changes in precipitation-evaporation balance) (Steinman and Abbott, 2012) (Figs. 4 and 8). It is possible, for example, that precipitation amounts during this time were less than statistically derived values, and that lake levels were correspondingly lower and $\delta^{18}O$ values were higher. The fact that both the CL and SL sediment cores are more enriched in oxygen-18 during this time supports this assertion.

Uncertainly in climate data does not, however, provide a potential explanation for the incoherence between measured and modeled $\delta^{18}O$ values over the 1980–2000 time period when precipitation amounts have much smaller prediction limits (Figs. 4 and 8). Likewise, dating uncertainties (which can explain offsets in the timing of isotopic shifts, but not the magnitude) do not provide a viable explanation given the smaller error range within the age models over this interval (Fig. 5). Possible explanations are that either the sediment $\delta^{18}O$ values are not reflective of water $\delta^{18}O$ values during this time, or that under certain lake sediment and water geochemical conditions (or climatic scenarios) the model fails to approximate reality. The first of these two explanations is perhaps the simplest, in that a small amount of mixing in the uppermost sediment likely occurred during core retrieval such that the temporal resolution of the core is lower than that of in situ sediment. This could explain only part of the disparity, however, given that the average modeled (−4.7‰ and −0.8‰, for CL and SL, respectively) and measured (−5.4‰ and −1.4‰) sediment $\delta^{18}O$ values over the 1980–2000 interval are considerably different. It is more likely, therefore, that the model predictions for this interval are incorrect. One possibility that is not accounted for is the incursion of air masses from the north that are more isotopically depleted (due to transcontinental rainout) than the much more common air masses from the west. This scenario would have produced rainfall that was more isotopically depleted along

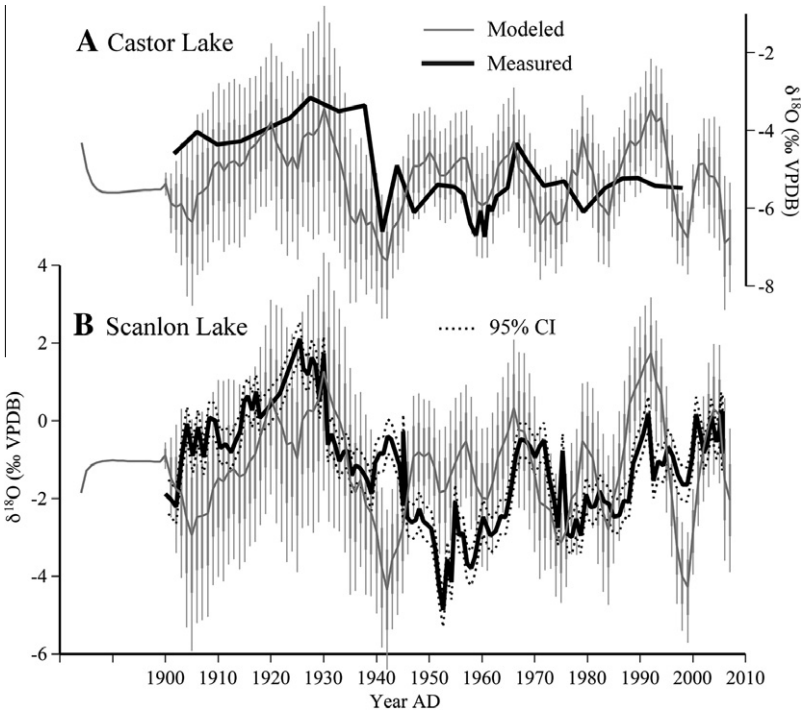

Fig. 9. Modeled (gray) and measured (black) aragonite $\delta^{18}O$ values for Castor Lake (A) and Scanlon Lake (B) from simulations with disabled temperature-precipitation $\delta^{18}O$ coupling. Thick and thin vertical gray lines depict the 1σ and 2σ prediction intervals, respectively, of 100 distinct simulations averaged to produce the modeled values. Five year averages of modeled data are shown. The fine dashed lines in (B) depict the confidence interval for $\delta^{18}O$ measurements of SL ostracods.

with correspondingly lower lake water and sediment $\delta^{18}O$ values. Another possibility lies in the potential for changes in the influence of temperature on the isotopic composition of precipitation. Several studies have shown that this assumed relationship (i.e., a shift of +0.6‰/°C) is not necessarily constant through time and that it can vary spatially (Rozanski et al., 1993; Johnson and Ingram, 2004; Schmidt et al., 2007), which could explain a large proportion of the disparity between the modeled and measured sediment $\delta^{18}O$ values. To test this idea, we conducted a series of simulations in which the temperature-precipitation $\delta^{18}O$ control algorithm was disabled (i.e., turned off). Results from these tests (Fig. 9) correlate more strongly to measured $\delta^{18}O$ values over the 1980–2000 interval but do not entirely explain the discrepancy, suggesting that either more isotopically depleted air masses or inaccuracy derived from some aspect of the lake-catchment model (or both) are the reason(s) for the differences.

In general, limitations in sediment core processing and dating as well as potential variation in the timing of carbonate mineral formation reduce the covariance between modeled and measured sediment core $\delta^{18}O$ values over shorter (i.e., subdecadal) time periods (Figs. 8 and 9). Further, uncertainty in climate data produces a range of possible realizations of modeled lake hydrologic and isotopic states rather than just one value for each time period (i.e., many possible depths and sediment $\delta^{18}O$ values exist for each year) making direct comparisons even more difficult. The generally strong coherence (within age model errors), however, between modeled and measured $\delta^{18}O$ values on decadal timescales demonstrates that over longer time periods, the model captures lake sediment isotopic variations with reasonable accuracy. This implies that sediment oxygen isotope records lacking annually (or nearly annually) resolved age control, cannot be expected to strongly covary with model isotopic predictions over the short term (i.e., 5–10 years) because of dating, climate data, and model uncertainties, but can be expected to covary over longer time periods when comparing averaged values.

4. CONCLUSIONS

We have demonstrated that lake-catchment models forced with continuous, instrumental climate data are capable of reproducing observed lake level changes and measured sediment $\delta^{18}O$ values on decadal timescales. This finding has important implications for the use of lake geochemical (i.e., isotope and ion) models in investigations of modern, future, and paleo lake responses to climate change. Of considerable importance to water management strategies, quantitative estimates of average, multidecadal hydroclimatic conditions spanning thousands of years could potentially be developed through model analyses of multidecadal (or longer) average sediment core $\delta^{18}O$ and δD values in lake systems for which modern climate and catchment data are available as model inputs (and for which catchment hydrology has not significantly changed, e.g., through stream piracy). Model simulations designed

to produce such solutions would have to include stochastic as well as mean state variations in the hydroclimatic variables and could be used to estimate, for example, past precipitation amounts within probabilistic limits defined by variance in the climatic variables and additional influences on the lake-catchment system (e.g., catchment vegetation on soil available water capacity or the effects of basin infill and morphology change through time). To successfully conduct such a study, however, several additional requirements should be met such as assessment of the relative influence of model initial conditions (i.e., lake hydrologic and isotopic states prior to the initiation of instrumental climatic data), piezometer studies of groundwater hydrology and geochemistry, and comparison of model derived, quantitative predictions of hydroclimatic variables to direct climatological observations (e.g., weather station data spanning multiple decades). In the second paper in this series (Steinman and Abbott, 2012), we address several of these issues and explore the potential of using lake sediment $\delta^{18}O$ records from CL to reconstruct seasonal precipitation amounts in north-central Washington.

ACKNOWLEDGEMENTS

We thank Jeremy Moberg, Chris Helander, Broxton Bird, and Jon Riedel for assistance in the field. Neil Tibert (University of Mary Washington) provided SEM images and identified ostracods. This work was funded by the US National Science Foundation AGS-PRF (AGS-1137750) and Paleo Perspectives on Climate Change (P2C2) programs.

APPENDIX A. SUPPLEMENTARY DATA

Supplementary data associated with this article can be found, in the online version, at http://dx.doi.org/10.1016/j.gca.2012.11.026.

REFERENCES

Abbott M. B. and Stafford T. W. (1996) Radiocarbon geochemistry of ancient and modern arctic lakes. *Baffin Island. Quaternary Res.* **45**, 300–311.

Appleby P. G. and Oldfield F. (1978) The calculation of lead-210 dates assuming a constant rate of supply of unsupported ^{210}Pb to the sediment. *Catena* **5**, 1–8.

Appleby P. G. and Oldfield F. (1983) The assessment of ^{210}Pb data from sites with varying sediment accumulation rates. *Hydrobiologia* **103**, 29–35.

Appleby P. G., Nolan P. J., Gifford D. W., Godfrey M. J., Oldfield F., Anderson N. J. and Battarbee R. W. (1986) ^{210}Pb dating by low background gamma counting. *Hydrobiologia* **143**, 21–27.

Benson L. and Paillet F. (2002) HIBAL: a hydrologic-isotopic-balance model for application to paleolake systems. *Quaternary Sci. Rev.* **21**, 1521–1539.

Binford M. W. (1990) Calculation and uncertainty of ^{210}Pb dates for PIRLA project sediment cores. *J. Paleolimnol.* **3**, 253–267.

Bowen G. J. and Revenaugh J. (2003) Interpolating the isotopic composition of modern meteoric precipitation. *Water Resour. Res.* **39**, 1299.

Curry B. B. (1999) An environmental tolerance index for ostracodes as indicators of physical and chemical factors in aquatic habitats. *Palaeogeogr. Palaeocl.* **148**, 51–63.

De Deckker P., Chivas A. R. and Shelley J. M. G. (1999) Uptake of Mg and Sr in the euryhaline ostracod *Cyprideis* determined from in vitro experiments. *Palaeogeogr. Palaeocl.* **148**, 105–116.

Dinçer T. (1968) The use of oxygen 18 and deuterium concentrations in the water balance of lakes. *Water Resour. Res.* **4**, 1289–1306.

Donovan J. J., Smith A. J., Panek V. A., Engstrom D. R. and Ito E. (2002) Climate-driven hydrologic transients in lake sediment records: calibration of groundwater conditions using 20th Century drought. *Quat. Sci. Rev.* **21**, 605–624.

Eugster H. P. and Jones B. F. (1979) Behavior of major solutes during closed-basin brine evolution. *Am. J. Sci.* **279**, 609–631.

Gat J. R. (1970) Environmental isotope balance of Lake Tiberias. In *Isotopes in hydrology*. IAEA. pp. 109–127.

Gibson J. J., Prepas E. E. and McEachern P. (2002) Quantitative comparison of lake throughflow, residency, and catchment runoff using stable isotopes: Modeling and results from a regional survey of Boreal lakes. *J. Hydrol.* **262**, 128–144.

Henderson A. K. and Shuman B. N. (2009) Hydrogen and oxygen isotopic compositions of lake water in the western United States. *Geol. Soc. Am. Bull.* **121**, 1179–1189.

Hodell D. A., Schelske C. L., Fahnenstiel G. L. and Robbins L. L. (1998) Biologically induced calcite and its isotopic composition in Lake Ontario. *Limnol. Oceanogr.* **43**, 187–199.

Hostetler S. and Benson L. (1990) Paleoclimatic implications of the high stand of Lake Lahontan derived from models of evaporation and lake level. *Clim. Dynam.* **4**, 207–217.

Hostetler S. W. and Benson L. V. (1994) Stable isotopes of oxygen and hydrogen in the Truckee River-Pyramid Lake surface-water system. 2. A predictive model of $\delta^{18}O$ and $\delta^{2}H$ in Pyramid Lake. *Limnol. Oceanogr.* **39**, 356–364.

Ito E. and Forester R. M. (2009) Changes in continental ostracode shell chemistry; uncertainty of cause. *Hydrobiologia* **620**, 1–15.

Johnson K. R. and Ingram B. L. (2004) Spatial and temporal variability in the stable isotope systematics of modern precipitation in China: implications for paleoclimate reconstructions. *Earth Planet. Sci. Lett.* **220**, 365–377.

Jones M. D., Leng M. J., Roberts N., Turkes M. and Moyeed R. (2005) A coupled calibration and modeling approach to the understanding of dry-land lake oxygen isotope records. *J. Paleolimnol.* **34**, 391–411.

Kelts K. and Hsu K. J. (1978) Freshwater carbonate sedimentation. In *Lakes – Chemistry, Geology, Physics* (ed. A. Lerman). New York, Heidelberg, Berlin. pp. 295–323.

Kim S. and O'Neil J. R. (1997) Equilibrium and nonequilibrium oxygen isotope effects in synthetic carbonates. *Geochim. Cosmochim. Acta* **61**, 3461–3475.

Kim S., O'Neil J. R., Hillaire-Marcel C. and Mucci A. (2007) Oxygen isotope fractionation between synthetic aragonite and water: influence of temperature and Mg^{2+} concentration. *Geochim. Cosmochim. Acta* **71**, 4704–4715.

Koschel R., Benndorf J., Proft G. and Recknagel F. (1983) Calcite precipitation as a natural control mechanism of eutrophication. *Arch. Hydrobiol.* **98**, 380–408.

Koschel R. (1997) Structure and function of pelagic calcite precipitation in lake ecosystems. *Verh. Internat. Verein. Limnol.* **26**, 343–349.

Nelson D. B., Abbott M. B., Steinman B. A., Polissar P. J., Stansell N. D., Ortiz J. D., Rosenmeier M. F., Finney B. P. and Riedel J. (2011) A 6000 year lake record of drought from the Pacific Northwest. *P. Natl. Acad. Sci. USA* **108**, 3870–3875.

Oldfield F. and Appleby P. G. (1984) Empirical testing of 210Pb-dating models for lake sediments. In *Lake Sediments and*

Environmental History (eds. E. Y. Haworth and W. G. Lund). University of Minnesota Press, Minneapolis, Minnesota. pp. 93–124.

Palacios-Fest M. R., Carreño A. L., Ortega-Ramirez J. R. and Alvarado-Valdéz G. (2002) A paleoenvironmental reconstruction of Laguna Babicora, Chihuahua, Mexico based on ostracode paleoecology and trace element shell chemistry. *J. Paleolimnol.* **27**, 185–206.

Raidt H. and Koschel R. (1988) Morphology of calcite crystals in hardwater lakes. *Limnologica* **19**, 3–12.

Reimer P. J., Baillie M. G. L., Bard E., Bayliss A., Beck J. W., Bertrand C. J. H., Blackwell P. G., Buck C. E., Burr G. S., Cutler K. B., Damon P. E., Edwards R. L., Fairbanks R. G., Friedrich M., Guilderson T. P., Hogg A. G., Hughen K. A., Kromer B., McCormac F. G., Manning S. W., Ramsey C. B., Reimer R. W., Remmele S., Southon J. R., Stuiver M., Talamo S., Taylor F. W., van der Plicht J. and Weyhenmeyer C. E. (2004) IntCal04 Terrestrial radiocarbon age calibration, 26–0 ka BP. *Radiocarbon* **46**, 1029–1058.

Rozanski K., Araguás-Araguás L. and Gonfiantini R. (1993) Isotopic patterns in modern global precipitation. In *Climate Change in Continental Isotopic Records* (eds. P. K. Swart, K. L. Lohmann, J. McKenzie, S. Savin). American Geophysical Union, Washington, DC. pp. 1–37.

Sanford W. E. and Wood W. (1991) Brine evolution and mineral deposition in hydrologically open evaporite basins. *Am. J. Sci.* **291**, 687–710.

Schelske C. L., Peplow A., Brenner M. and Spencer C. N. (1994) Low-background gamma counting: applications for ^{210}Pb dating of sediments. *J. Paleolimnol.* **10**, 115–128.

Schmidt G. A., LeGrande A. N. and Hoffmann G. (2007) Water isotope expressions of intrinsic and forced variability in a coupled ocean–atmosphere model. *J. Geophys. Res. Atmos.* **112**. http://dx.doi.org/10.1029/2006JD007781.

Shapley M. D., Ito E. and Donovan J. J. (2005) Authigenic calcium carbonate flux in groundwater-controlled lakes: implications for lacustrine paleoclimate records. *Geochim. Cosmochim. Acta* **69**, 2517–2533.

Shapley M. D., Ito E. and Donovan J. J. (2008) Isotopic evolution and climate paleorecords: modeling boundary effects in groundwater-dominated lakes. *J. Paleolimnol.* **39**, 17–33.

Smith A. (1993) Lacustrine ostracodes as hydrochemical indicators in lakes of the north-central United States. *J. Paleolimnol.* **8**, 121–134.

Sondi I. and Juracic M. (2010) Whiting events and the formation of aragonite in Mediterranean karstic marine lakes: new evidence on its biologically induced inorganic origin. *Sedimentology* **57**, 85–95.

Steinman B. A., Rosenmeier M. F., Abbott M. B. and Bain D. J. (2010a) The isotopic and hydrologic response of small, closed-basin lakes to climate forcing from predictive models: application to paleoclimate studies in the upper Columbia River basin. *Limnol. Oceanogr.* **55**, 2231–2245.

Steinman B. A., Rosenmeier M. F. and Abbott M. B. (2010b) The isotopic and hydrologic response of small, closed-basin lakes to climate forcing from predictive models: simulations of stochastic and mean-state precipitation variations. *Limnol. Oceanogr.* **55**, 2246–2261.

Steinman B. A., Abbott M. B., Mann M. E., Stansell N. D. and Finney B. P. (2012) 1500 year quantitative reconstruction of winter precipitation in the Pacific Northwest. *P. Natl. Acad. Sci. USA* **109**, 11619–11623.

Steinman B. A. and Abbott M. B. (2012) Isotopic and hydrologic responses of small, closed lakes to climate variability: Hydroclimate reconstructions from lake sediment oxygen isotope records and mass balance models. *Geochim. Cosmochim. Acta*, **105**, 342–359.

Stuiver M., Reimer P. J. and Braziunas T. F. (1998) High-precision radiocarbon age calibration for terrestrial and marine samples. *Radiocarbon* **40**, 1127–1151.

Thompson J. B., Schultze-Lam S., Beveridge T. J. and Des Marais D. J. (1997) Whiting events: Biogenic origin due to the photosynthetic activity of cyanobacterial picoplankton. Limnol. Oceanogr. **42**, 133–141.

von Grafenstein U., Erlernkeuser H. and Trimborn P. (1999) Oxygen and carbon isotopes in modern fresh-water ostracod valves: assessing vital offsets and autecological effects of interest for paleoclimate studies. *Palaeogeogr. Palaeocl.* **148**, 133–152.

Associate editor: Josef P. Werne